5-2018

Analysis of Biological Response to ECM Hydrogel Injection

Grady Dunlap
University of Arkansas, Fayetteville

Analysis of Biological Response to ECM Hydrogel Injection

An Undergraduate Honors College Thesis

in the

Department of Biomedical Engineering

College of Engineering

University of Arkansas

Fayetteville, AR

By

Grady Dunlap

Table of Contents

Abstract

Under normal circumstances, skeletal muscle possesses the capacity to regenerate and heal via inflammatory and myogenic pathways. In cases of severe tissue loss or certain diseases, this capacity is lost, often resulting in loss of tissue function. Extracellular matrix (ECM), the protein scaffold which houses cells in physiological tissue, has been shown to have structural and chemical properties which influence cell migration and phenotype. This results in ECM's capacity to encourage a regenerative response when implanted into severely damaged skeletal muscle. Additional advantages are apparent when an ECM scaffold is digested into a hydrogel, namely less invasive implantation via injection and the ability to better fill the injury cavity. While indications of therapeutic potential of ECM hydrogels are appearing, a greater understanding of their effect on skeletal muscle is necessary. This study investigated the impact of ECM hydrogel injection on skeletal muscle both as whole, functional tissue and at the genetic expression of the inflammatory and myogenic regenerative pathways. Rats were given five 0.1mL injections of saline in one tibialis anterior muscle (TA) and five 0.1mL injections of ECM hydrogel in the other TA. At timepoints of three days and two weeks, force measurements were taken and TAs were harvested. Gross TA morphology revealed no consistent difference between treatments, and peak force measurements averaged and normalized to body mass showed a decrease in force-creating potential in the ECM hydrogel TAs. qRT-PCR was performed, targeting inflammatory expression of IL-6 and IL-10 and myogenic expression of Pax7, MyoD, and myogenin (MyoG). While data was limited by small sample sizes and lack of statistical significance, results suggested a short-term inflammatory and myogenic response by the ECM hydrogel injections. Future studies would need to use larger sample sizes to produce statistically significant data to further explore these indicated results.

1. Introduction

Under the diverse demands of movement and force production required of it, skeletal muscle is prone to injury and disease which hinder its ability to perform necessary function. Like much of the tissue in the body, skeletal muscle has the remarkable ability to repair itself under normal circumstances via inherent inflammatory and myogenic pathways.[1,2]

In the broadest sense, the inflammatory pathway is the immune system's method of fighting off harmful factors and ensuring homeostasis resumes.[3] Skeletal muscle is essentially a vast bundle of myofibers, and when injury causes a tear or rupture in these myofibers, inflammatory cells release pro-inflammatory cytokines, such as interleukin 6 (IL-6) ,[3,4] to recruit monocytes, which then differentiate into macrophages. These macrophages are essential in removing invasive agents or necrotic myofibers and muscle tissue,[5,6] but it is essential that they are held in check by a balance of anti-inflammatory cytokines, such as interleukin 10 (IL-10),[3,4] and the cells they recruit to prevent too much catabolism.[4]

The myogenic pathway comprises of the actual process of skeletal muscle regeneration and repair via the formation of new myofibers. Responding to damage, dormant satellite cells are activated and begin to divide and differentiate into myocytes, which then fuse into new myofibers and reintegrate into the whole tissue.[1,2,7] This activation of satellite cells is caused by transcription factor Pax7,[7,8,9] while their proliferation and differentiation and then continued differentiation and tissue integration are largely due to the protein, MyoD,[9,10,11] and transcription factor, myogenin (MyoG),[9,11] respectively.

These inflammatory and myogenic regenerative mechanisms occur under normal conditions to result in recovery. However, massive loss of tissue and certain muscle degenerative diseases can

prevent these processes from functioning properly, leading to buildup of scar tissue or loss of skeletal muscle function.[1,2] This level of heavy tissue loss can result not uncommonly from traumatic accidents, surgical removals of tumors, muscular dystrophies, and injuries sustained during combat.[2] Unfortunately, even when amputation is avoided, often the best treatment for such injury consists of replacing the obsolete skeletal muscle tissue with still functioning muscle from elsewhere, an invasive procedure that still results in scar tissue.[2] Therefore, there is great interest in a means of more effective regeneration and repair of severely damaged skeletal muscle.

Organs and tissue are made of cells arranged within a complex scaffold of macromolecules called the extracellular matrix (ECM). ECM is composed largely of type I collagen as well as elastin and fibronectin, which provide structural support and strength, the ability to recover elastically, and the capacity for cell attachment and migration, respectively. Additional major components include proteoglycans (PGs) and glycosaminoglycans (GAGs), which account for ECM's ordered structure and ability to interact with functional molecules such as growth factors and cytokines.[2,8] Many of these functional molecules are secreted by cells housed within ECM, resulting in a structure, molecular composition, and functional molecular arrangement uniquely optimized for the ECM's native tissue.[12]

This structural and molecular functionality result in ECM's capacity to support a cellular and tissue growth response in numerous tissue types, particularly skeletal and cardiac muscle, particularly due to its influence on cell behavior, migration, and phenotype.[1,6,12,13,14] This has led to much interest in the therapeutic potential of ECM as an implantable scaffold into severely damaged skeletal muscle. Importantly, implanted ECM is able to be degraded by inflammatory response,[6] which in vitro studies have shown releases many of its housed growth factors,

resulting in the recruitment of additional myogenic cells and promotion of anti-inflammatory macrophages.[2,5] Additionally, ECM from different native tissue types can be selected purposefully for implantation to induce differing responses,[1,6,14] such dermal tissue ECM degrading faster than urinary bladder ECM and indicating a stronger myogenic response.[1] For even further procedural specification, ECM can be seeded artificially with additional functional molecules or cells, such as stem cells to encourage desired tissue growth[5] or AG-doped bioactive glass to inhibit unwanted growth of certain bacterial species.[13]

Of even greater therapeutic interest is the use of ECM digested into a hydrogel. While largely retaining the potential for application as a scaffold of its intact counterpart,[1,6,14,15] an ECM hydrogel offers the major benefits of being injectable to allow for far less invasive delivery[6,12] and the ability to, as a liquid, fill the injury cavity regardless of shape irregularity.[1,6] This more precise delivery allows for application on tissue types into which intact ECM scaffold cannot be implanted, such as potential treatment for peripheral artery disease.[10] While synthetic hydrogels also offer this delivery advantage, an ECM hydrogel doesn't need to be seeded with growth and adhesion promoting molecules.[6] Finally, an ECM hydrogel offers the potential for more a more controlled release of cells, drugs, or other bioactive molecules to the injury site.[1,6]

While ECM hydrogels offer much promise as an injectable scaffold for skeletal muscle regeneration, much of the direct impact of the injection of an ECM hydrogel in vivo is not yet well understood. ECM hydrogel has been indicated by histological evidence as a myogenic promoter in vivo,[6] and in vitro tests have indicated recruitment of MyoD-positive cells for cultured damaged skeletal muscle on hydrogel scaffolds[10] and increased Pax7 and MyoD expression from murine embryonic stem cells cultured on collagen hydrogel matrix.[8] There is evidence to support ECM hydrogel injection as a means to elicit a myogenic response in skeletal

muscle, but further work needs to be done to fully understand its overall regenerative effect on skeletal muscle.

This study investigates the direct impact of ECM hydrogel injection on skeletal muscle on the macroscale functional level and specifically on the inflammatory and myogenic pathways. Skeletal muscle ECM (sECM) was digested into a hydrogel and injected into the hind leg tibialis anterior muscle (TA) of rats to be compared with an injected saline control in the other hind leg TA. Timepoints were set at three days and two weeks to allow for short- and middle-term timepoint comparison. Macroscale functional comparison was performed by examining gross morphology of TAs and force production potential of the different hind legs at the end of the timepoints. Impact on the myogenic and inflammatory pathways was investigated by performing qRT-PCR on samples of the TAs to compare expression of Pax7, MyoD, and MyoG for myogenic analysis and expression of IL-6 and IL-10 for inflammatory analysis. Better understanding of these ECM hydrogel effects are essential for further exploration of the therapeutic potential of this scaffold-delivery method.

2. Materials and Methods

2.1 Reagents. Sodium dodecyl sulfate (SDS) was purchased from Amresco (Solon, OH). Dulbecco's Phosphate Buffered Saline (PBS, 1X) was purchased from Gibco (Grand Island, NY). Deoxyribonuclease I (DNase, bovine pancreas) was purchased from Sigma Aldrich (St. Louis, MO). Ribonuclease A (RNase) was purchased from Thermo Fisher Scientific (Carlsbad, CA). Penicillin/streptomycin (PenStrep, 10,000units/mL Penicillin, 10,000ug/mL Streptomycin) was purchased from Gibco (Grand Island, NY). Pepsin (porcine gastric mucosa) was purchased from Sigma Aldrich (St. Louis, MO). Trizol was purchased from Thermo Fisher Scientific (Carlsbad, CA). An Ambion Purelink RNA Mini Kit was purchased from Thermo Fisher

Scientific (Carlsbad, CA). Choloform was purchased from Alpha Aesar (Tewksbury, MA).

RNase-free water was purchased from Thermo Fisher Scientific (Carlsbad, CA). SuperScript

VILO was purchased from Thermo Fisher Scientific (Carlsbad, CA). Taqman MasterMix was

purchased from Thermo Fisher Scientific (Carlsbad, CA). Housekeeping gene 18s, Pax7, MyoD,

MyoG, IL-6, and IL-10 PCR gene targets were purchased from Thermo Fisher Scientific

(Carlsbad, CA).

2.2 Preparation of ECM Gel

2.2.1 ECM From Harvested Tissue. A decellularization solution of 1% SDS in 10mM Tris-

HCl, 1% EDTA buffer was prepared, and human skeletal muscle samples were trimmed of

excess fascia and cut into ≈1cm cubic pieces. The resulting 84.58g of tissue was placed in

250mL of sterile-filtered SDS solution at room temperature and undergoing gentle rocking

agitation. Twice a week for one month, the used SDS solution was removed and replaced with

new sterile-filtered SDS solution. Tissue considered fully decellularized once visually clear and

white, with no traces of pink or yellow remaining (see Figure 1). Once fully decellularized, all

subsequent tissue transfers occur in biosafety sterile cabinet, beginning with three 24-hour sterile

1% PBS rinses, all at 4°C.

A DNase/RNase digestion solution was prepared by creating a buffer solution of 10mM Tris-

HCl, 2.5mM $MgCl_2$, and 0.5mM $CaCl_2$ in DI and adding 1kU/mL DNase and 20U/mL RNase.

300mL of this solution was then sterile-filtered and used for a 24-hour rinse of the tissue at 4°C.

This rinse was followed by three additional sterile 1% PBS rinses, each for 24 hours at 4°C. A

solution of 1% PenStrep in DI was created, and a single 24-hour rinse was performed at 4°C. The

tissue was then rinsed three times in DI, each for 24 hours at 4°C. The tissue was then lyophilized in DI and stored at -20°C.

2.2.2. ECM Digestion. In a sterile biosafety cabinet, lyophilized skeletal muscle ECM (sECM) tissue was minced to increase surface area, then returned to -20°C storage. Two samples of ≈100mg were measured and placed in sterile scintillation vials (see Figure 1). 0.5L of 0.1M HCl was prepared and adjusted to a pH of 2.1. A pepsin digestion solution was created at a concentration of 10mg/mL by adding 500mg of lyophilized pepsin to 50mL of the HCl. In a sterile biosafety cabinet, the resulting 50mL of digestion solution was sterile-filtered added to each sECM tissue vial at 15mg ECM/mL solution. A stir bar was placed in each vial, and both were stirred at 400rpm at room temperature for 48 hours (see Figure 1). The resulting pre-gel solutions were then pH-adjusted to a physiological pH of 7.4 using the addition of 0.1M NaOH. This finished ECM hydrogel was then drawn into 1mL syringes, sealed in autoclave bags to maintain sterility, and placed in -20°C storage.

2.3 ECM Injection Procedure. Surgical and collection procedures were in accordance with IUCAC protocol number 18055. Eight rats (all male, strain SD, three to four months old) were designated sECM 5 through sECM 12, with sECM 5 through sECM 8 assigned the two-week group and sECM 9 through sECM 12 assigned the three-day group. Each rat was administered isoflurane at 4% via inhalation to render unconsciousness, weighed, placed on a heating pad, and administered isoflurane at 2% via inhalation to maintain unconsciousness. Hind legs were shaved and sanitized with iodine to expose the skin so that the tibialis anterior muscle on each hind leg could be located. On each tibialis anterior muscle, five dots were placed to mark injection sites (see Figure 2).

On the right TA of each rat, five intramuscular injections of 0.1mL of sterile PBS were delivered, one injection of each of the marked dots for a total dose of 0.5mL. This same methodology was used with prepared sECM hydrogels on the left TA of each rat (see Figure 3). Following injections, each rat was given a subcutaneous 0.1mL injection of 0.3mg/mL buprenorphine and half of a 2mg carprofen tablet and returned to a new cage. Rats were given additional subcutaneous 0.1mL injection of 0.3mg/mL buprenorphine injection at 12 hours and half of a 2mg carprofen tablet daily for three days afterward.

2.4 Tissue and Data Collection Procedures

2.4.1. Force Data Collection Procedure. After three days, rats sECM 9 through sECM 12 were individually administered isoflurane at 4% via inhalation to induce unconsciousness, weighed, and placed by a force plate, and administered isoflurane at 2% via inhalation to maintain unconsciousness. Individually, each hind foot of each rat was taped to the force plate, with two electrodes inserted into the TA muscle of that leg. Using probes, the muscle was electrically stimulated to produce a kick, the force of which was recorded (see Figure 4 and Figure 5).

2.4.2. Tissue Collection Procedure. After force measurements were taken, each rat was placed on a heating pad while isoflurane was administered continuously at 2% via inhalation. The TA of each hind leg was harvested, weighed, photographed, cut into segments, and frozen for storage (see Figure 6). One segment of each harvested TA was designed for PCR testing. After harvest, each rat was sacrificed using carbon dioxide in accordance with protocol. All animal weight and force data was compiled into a spreadsheet for record-keeping.

2.4.3. qRT-PCR. Tissue samples saved for PCR were individually, while frozen, placed in 1mL of Trizol reagent and homogenized using 3 to 5 cycles of 3 to 5 seconds in Polytron mechanical

grinder. Fully-homogenized samples were then pipetted into labeled Eppendorf tubes and stored at -80°C (see Figure 7).

Homogenized samples were thawed in an ice bath, and 200uL chloroform was added to each. Samples were mixed using a vortex mixer for 15 seconds, allowed to sit for 3 minutes, then mixed again for 15 seconds. Samples were centrifuged for 25 minutes at 15,000rpm at 4°C, resulting in separation of the samples into protein, DNA, and RNA layers (see Figure 7). For each sample, the top, clear layer containing the RNA was pipetted into a new Eppendorf tube while avoiding contact or contamination from the middle DNA and bottom protein layers, which were discarded. The volume of RNA solution obtained for each sample was noted, and equal volume of 70% DEPC EtOH was added to each. Samples were transferred to Ambion kit RNeasy spin columns and centrifuged for 30 seconds at 15,000rpm. Flow-through was discarded, and samples underwent three rinses: one with 700uL of Ambion kit Wash Buffer 1 and then two with 500uL of Ambion kit Wash Buffer II. For each of the wash buffer rinses, the samples were centrifuged for 15 seconds at 15,000rpm with flow-through discarded. After sitting for 1 minutes, samples were centrifuged for 1 minute at 15,000rpm. Spin columns were transferred to recovery Eppendorf tubes, and 20uL of RNase-free water was added to each column. After sitting for 2 minutes, samples were centrifuged for 1 minute at 15,000rpm. This final flow-through was the isolated RNA in water. RNA quantification was performed by running two 2uL of each sample's thawed, isolated RNA solution on a reader plate using Gen5 software, with each sample's RNA concentrations (two values were read for each) saved to a spreadsheet. Each sample was then labeled and stored at -80°C.

Isolated RNA samples were thawed in an ice bath. Using the average of the two quantification values for each sample's ng RNA per uL solution, the volume of solution to contain 1ug RNA

was calculated. This calculated volume for each RNA sample was then pipetted into an Eppendorf tube, with RNase-free water added to achieve a total volume of 8uL for each sample. To each sample, 1uL of DNase I, 1uL of DNase buffer, 4uL of SuperScript VILO Master Mix, and 6uL of RNase-free water were added. Samples were loaded into a computer plate reader, and reverse transcriptase was performed. The resulting in cDNA samples were stored at -20°C.

cDNA samples were thawed and diluted down to 1:100 solutions using RNase-free water. For PCR, each sample was run with six gene targets: 18s housekeeping gene, Pax7, MyoD, myogenin, IL-6, and IL-10. With n=sample size for a single 48-well plate, a target mix was prepared for each target gene according to Equation 1:

$$(n + 1.5) \cdot 12.5 = uL \; Taqman \; MasterMix$$

$$(n + 1.5) \cdot 1.25 = uL \; water$$

$$(n + 1.5) \cdot 1.25 = uL \; gene \; target$$

This target mix was then be mixed using the vortex mixer for 5 seconds. On the 48-well plate, in each designated well, 15uL of the target mix and 10uL of the sample 1:100 cDNA were added. The well plate was sealed with plastic and spun, and the plate and its designated layout were entered into the plate reader. PCR was performed, and the data was saved to a spreadsheet.

2.5 Statistical Analysis. Using Microsoft Excel, a Student's two-tail homoscedastic t-test for each data set was performed. Any asterisk on a figure indicates a resulting $p < 0.05$ value for that corresponding data.

3. Results

3.1 Peak Force Values. The peak force value from each measurement was determined, and the highest value from all measurements from one leg of one animal become the representative peak force value for that sample. Each peak value was normalized to the terminal whole-body mass of the animal. These values are displayed in Figure 4. These values were then grouped by leg and timepoint, and an average value was determined for each. These values are displayed in Figure 5.

3.2 Gross TA Morphology. After harvest, each TA was weighed and photographed. Representative samples from each group and timepoint are shown in Figure 5.

3.3 qRT-PCR Results. PCR data is presented as the left TA values in reference to the right TA values, the ECM group in reference to the control. For each target gene, the difference between the target gene and housekeeping gene's values were calculated, averaged, and referenced to the average difference of the control group. These values were then used as a negative exponent of 2 and were then normalized to that average control group value. These resulting values were then averaged for both groups, resulting in a control value of 1 and an ECM leg value in reference to that control. This calculation was performed separately for each gene and for each timepoint, and each ECM value was graphed in reference to its corresponding control. The resulting graphs for Pax7 are shown in Figure 8. The resulting graphs for MyoD are shown in Figure 9. The resulting graphs for MyoG are shown in Figure 10. The resulting graphs for IL-6 are shown in Figure 11. The resulting graphs for IL-10 are shown in Figure 12.

4. Discussion

4.1 Peak Force Values. As shown in Figure 5, both after three days and after two weeks, on average, higher peak forces were achieved by the PBS control TAs than those of the sECM TAs. While the standard deviation is also higher on the control TAs, it was unexpected that the higher

force-creating potential would result in this group. As shown in Figure 4, sECM 6 is an outlier in the data with a much greater peak force value and likely exaggerated the two-week control TA group average, but the three-day group is fairy consistent with the control TAs producing higher peak forces. This could indicate an overall weakening of the tissue at a functional level caused by the sECM injections, whether due to increased myogenic or inflammatory activity changing the structure within the skeletal muscle or due to a decreased response compared to the PBS control. It may also simply be due to the inconsistency of the force measurement itself, and it should be noted that there is an absence of statistical significance. Overall, higher forces were achieved after two weeks, which is to be expected due to the longer recovery time, but this may indicate that some form of recovery was still occurring at three days, meaning that myogenic and inflammatory pathways were likely activated to at least some extent in both TA groups.

4.2 Gross TA Morphology. As shown in Figure 6, virtually no difference is seen between the PBS control TAs and the sECM TAs. Because the extent of the injury caused by the injection procedure was minimal and consistent to both groups, this overall similar result is to be expected.

4.3 Pax7. As shown in Figure 8, at the end of the three-day timepoint, comparison between the PBS control and sECM TAs shows a higher rate of Pax7 expression in the sECM TAs, though with a larger standard deviation. At the end of the two-week timepoint, the sECM TAs is much more similar to the control in both expression and standard deviation, with the Pax7 expression being slightly higher in the control leg. Because Pax7 plays a role in the activation of the satellite cells at the beginning of the myogenic pathway,[7,8,9] it makes sense for Pax7 expression to be increased after three days rather than two weeks. It should be noted that the data is based on small sample size and that the data is not statistically significant based of Student's t-testing, but

based on the results, a higher degree of expression indicates a stronger initial myogenic response in the sECM subjects after three days.

4.4 MyoD. As shown in Figure 9, at the end of the three-day timepoint, comparison between the PBS control and sECM TAs shows only a slightly higher rate of MyoD expression in the sECM TAs along with a higher standard deviation. At the end of the two-week timepoint, the sECM TAs show half the expression of MyoD as the control TAs. Because MyoD expression follows Pax7 expression in the myogenic pathway, indication that activated satellite cells have begun growth and differentiation,[9,11] and because Pax7 expression indicated satellite cell activated had occurred to some extent, the relatively small increase in MyoD expression seems to indicate either a very early point in myogenic response to sECM injection at three days (not enough satellite cells activated for a strong proliferation or differentiation to begin) or a later point in myogenic response (differentiation of satellite cells nearing completion). If the sECM encouraged myogenesis, MyoD expression is either ahead or behind the point of the process at three days. Once again, the data is limited by the low sample size, and the absence of statistical significance should be noted.

4.5 MyoG. As shown in Figure 10, at the end of the three-day timepoint, comparison between the PBS control and sECM TAs shows a much higher expression of MyoG in the sECM TAs, along with a much higher standard deviation. At the end of the two-week timepoint, MyoG expression in the sECM TAs is virtually the same, though slightly lower, than that of the control TAs. Because MyoG indicates the nearing completion of the myogenic process, the final differentiation and integration of myoblasts into myofibers, and would be expressed after MyoD,[9,11] it is unexpected to see such a large amount of relative MyoG expression in sECM TAs as early as three days when Pax7 and MyoD expression was much more level between the

groups. This may be an indication that sECM injection encouraged a myogenic response and that the pathway ran to or near completion rather quickly after just over three days, perhaps due to the low severity of the injury caused by the procedure. Any myogenic activity caused by the sECM seems to have been long completed by the two-week timepoint, as none of the myogenic expression tests show much difference between the control and sECM TAs or a heightened expression by either after that much time had passed. Once again, the data is limited by the low sample size, and the absence of statistical significance should be noted.

4.6 IL-6. As shown in Figure 11, at the end of the three-day timepoint, comparison between the PBS control and sECM TAs shows a much higher expression of IL-6 in the sECM TAs, along with a higher standard deviation. At the end of the two-week timepoint, IL-6 expression in the sECM TAs is slightly smaller than that of the control TAs. As was the case with the myogenic results, any response to the sECM injections seems to have run its course by two weeks afterwards. Because IL-6 is a pro-inflammatory cytokine,[4] this heightened expression compared to the control may indicate a more traumatic effect by the introduction of sECM compared to PBS, but this increase may also indicate degradation of the sECM scaffold, an important occurrence in the inflammatory pathway encouraging myogenic response.[2,5,6] Once again, the data is limited by the low sample size, and the absence of statistical significance should be noted.

4.7 IL-10. As shown in Figure 12, at the end of the three-day timepoint, comparison between the PBS control and sECM TAs shows a much higher expression of IL-10 in the sECM TAs, along with a much higher standard deviation. At the end of the two-week timepoint, IL-10 expression in the sECM TAs is higher than that of the control TAs, the only gene target with higher expression at two weeks in the sECM TAs. Interestingly, at three days, the relative expression in the sECM TAs of IL-6 and IL-10 is quite similar. IL-10 is an anti-inflammatory cytokine, and

the inflammatory pathway is dependent on the balance of these pro- and anti-inflammatory cytokines. The ratio of IL-6 to IL-10 expression can be used as an indicator of overall activation of the pathway, and anti-inflammatory response is triggered by the presence of a pro-inflammatory response.[4] At three days, IL-6 and IL-10 expression levels in sECM TAs are nearly equal in reference to the control TAs. Such elevated IL-10 expression could indicate that at three days, the inflammatory pathway has run its course and balanced itself out, which would support the indication of a myogenic response being already underway at three days. Because myogenic data indicated that pathway too nearing completion, this timeline would make sense. If sECM injection indeed resulted in a greater myogenic and inflammatory response than that of the PBS injection, it is indicated that both response pathways were at or nearing completion after three days. Once again, the data is limited by the low sample size, and the absence of statistical significance should be noted.

5. Conclusions

This study sought to investigate the biological response to sECM hydrogel injection into skeletal muscle when compared to a saline control. This biological response was to be explored in the areas of gross morphology, functionality of the muscle, and the inflammatory and myogenic pathways. No consistent difference in effect on the gross morphology of the TA could be determined between sECM and PBS, and sECM injections actually resulted in less force-creating potential from the TAs when compared to the control. While the data in this study was limited by small sample size and absence of statistical significance, the results indicated a greater myogenic and inflammatory response in the sECM TAs than the PBS control TAs. The large MyoG expression, modest MyoD expression, and balanced IL-6 and IL-10 expressions at three days in the sECM TAs suggest both pathways had run to or near completion by tissue harvest at three

days, suggesting a potential for short-term sECM stimulation of these regenerative pathways, which would be a positive indication of the therapeutic potential of an ECM hydrogel.

Additional studies are required to more properly establish a foundational understanding of the direct biological and regenerative responses of ECM hydrogel introduction into skeletal muscle. This study utilized a very small sample size, likely heavily contributing to the lack of statistically significant data. For any of the indicated results to be considered more legitimate, more testing with significant data is necessary. Going beyond the immediate impacts, a key focus of future studies needs to be biological response to an ECM hydrogel injection to an injury. Studies are already underway on the therapeutic effects of ECM hydrogel on shoulder cuff defect repair in rabbits. From there, the effects of added molecular or chemical elements to the hydrogel on improved therapeutic response should be a focus.

6. Acknowledgements

7. References

1. Lev, R., Seliktar, D. Hydrogel biomaterials and their therapeutic potential for muscle injuries and muscular dystrophies. Journal of the Royal Society Interface [Internet] 2018 [cited 18 April 2018];15(138):20170380. Available from: https://www.ncbi.nlm.nih.gov/pmc/articles/PMC5805959/

2. Fuoco C, Petrilli LL, Cannata S, Gargioli C. Matrix scaffolding for stem cell guidance toward skeletal muscle tissue engineering. Journal of Orthopaedic Surgery and Research [Internet]. 2016 [cited 18 April 2018];11:86. Available from: https://www.ncbi.nlm.nih.gov/pmc/articles/PMC4962357/

3. Hélio J, Bruno B, Tiego A, et al. Inflammatory Mechanisms Associated with Skeletal Muscle Sequelae after Stroke: Role of Physical Exercise. Mediators of Inflammation [Internet]. 2016 [cited 21 April 2018];2016:19. Available from: https://www.hindawi.com/journals/mi/2016/3957958/

4. Sapan HB, Paturusi I, Jusuf I, et al. Pattern of cytokine (IL-6 and IL-10) level as inflammation and anti-inflammation mediator of multiple organ dysfunction syndrome (MODS) in polytrauma. International Journal of Burns and Trauma [Internet]. 2016 [cited 21 April 2018];6(2):37-43. Available from: https://www.ncbi.nlm.nih.gov/pmc/articles/PMC4913232/

5. Sicari B, Dziki J, Badylak S. Strategies for functional bioscaffold-based skeletal muscle reconstruction. Letter to the Editor: McGowan Institute for Regenerative Medicine, Department of Surgery, Department of Bioengineering, University of Pittsburgh, Pittsburgh, PA, USA [Internet]. 2015 [cited 18 April 2018];3(17). Available from: http://atm.amegroups.com/article/view/7951/8762

6. Wolf MT, Daly KA, Brennan-Pierce EP, et al. A Hydrogel Derived From Decellularized Dermal Extracellular Matrix. Biomaterials [Internet]. 2012 [cited 16 October 2017];33(29):7028-7038. Available from: https://www.ncbi.nlm.nih.gov/pmc/articles/PMC3408574/

7. Von Maltzahn J, Jones AE, Parks RJ, Rudnicki MA. Pax7 is critical for the normal function of satellite cells in adult skeletal muscle. Proceedings of the National Academy of Sciences of the United States of America [Internet]. 2013 [cited 18 April 2018];110(41):16474-16479. Available from: https://www.ncbi.nlm.nih.gov/pmc/articles/PMC3799311/

8. Kuraitis D1, Ebadi D, Zhang P, et al. Injected matrix stimulates myogenesis and regeneration of mouse skeletal muscle after ischaemic injury. European Cells and Materials [Internet]. 2012 [cited 18 April 2018];12(24):175-195. Available from: https://www.ncbi.nlm.nih.gov/pubmed/22972509

9. Pestronk, Alan. Myogenesis & Muscle Regeneration. WU Neuromuscular. Washington University [Internet]. 2018 [cited 21 April 2018]; Available from: https://neuromuscular.wustl.edu/mother/myogenesis.html

10. DeQuach JA, Lin JE, Cam C, et al. Injectable skeletal muscle matrix hydrogel promotes neovascularization and muscle cell infiltration in a hindlimb ischemia model. European cells & materials [Internet]. 2012 [cited 18 April];23:400-412. Available from: https://www.ncbi.nlm.nih.gov/pmc/articles/PMC3524267/

11. Halevy O, Piestun Y, Allouh, MZ, et al. Pattern of Pax7 expression during myogenesis in the posthatch chicken establishes a model for satellite cell differentiation and renewal. Developmental Dynamics [Internet]. 2004 [cited 21 April 2018];231(3):489-502. Available from: https://onlinelibrary.wiley.com/doi/full/10.1002/dvdy.20151

12. Badylak S, Freytes D, Gilbert T. Extracellular matrix as a biological scaffold material: Structure and function. Acta Biomaterialia [Internet]. 2009 [cited 16 October 2017];5(2009):1-13. Available from: http://rethinkhealing.com/wp-content/uploads/2013/02/Badylak_ActaBiomat_2009.pdf

13. Wang YY, Chatzistavrou1 X, Faulk D, et al. Biological and Bactericidal Properties of AG-Doped Bioactive Glass In A Natural Extracellular Matrix Hydrogel With Potential Application In Dentistry. European Cells and Materials [Internet]. 2015 [cited 16 October 2017];29(2015):342-355. Available from: http://www.ecmjournal.org/papers/vol029/pdf/v029a26.pdf

14. Freytes D, Martin J, Velankar S, et al. Preparation and rheological characterization of a gel form of the porcine urinary bladder matrix. Biomaterials [Internet]. 2008 [cited 16 October 2017];29(11):1630-1637. Available from: https://www.sciencedirect.com/science/article/pii/S0142961207010423?via%3Dihub

15. Seif-Naraghi SB, Salvatore MA, Schup-Magoffin PJ, et al. Design and Characterization of an Injectable Pericardial Matrix Gel: A Potentially Autologous Scaffold for Cardiac Tissue Engineering. Tissue Engineering Part A [Internet]. 2010 [cited 16 October 2017];16(6):2017-2027. Available from: https://www.ncbi.nlm.nih.gov/pmc/articles/PMC2949214/
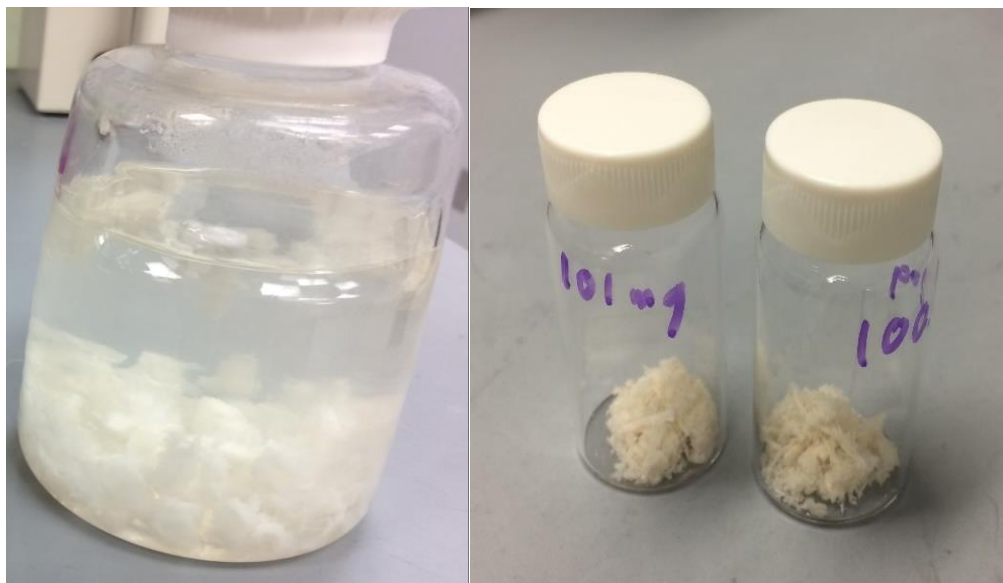
Figure 1 displays three of the main stages of ECM hydrogel preparation. Samples were decellularized (top left), lyophilized and minced (top right), and digested to a pre-gel solution (bottom).
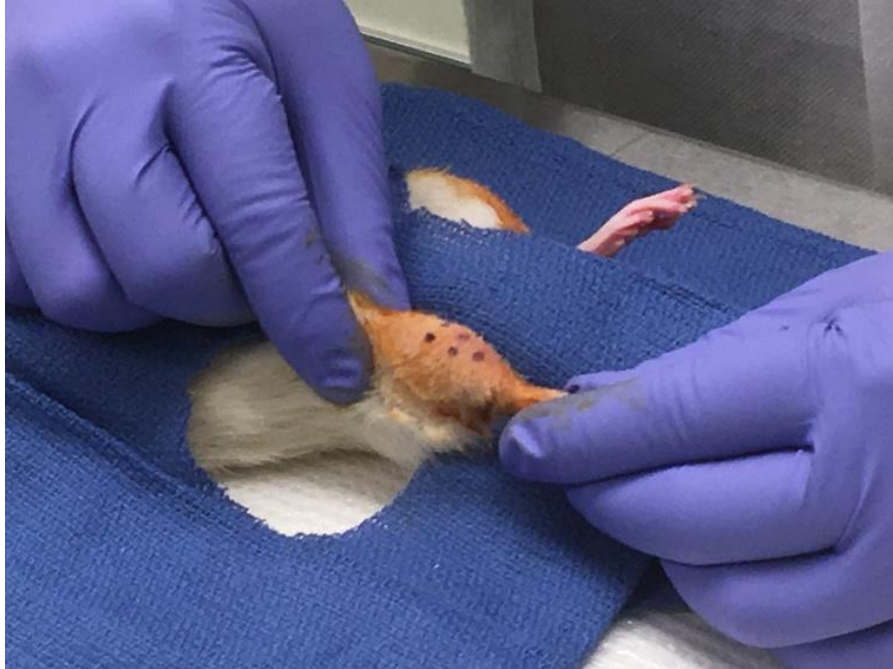
Figure 2 displays the 5 dots marked onto the skin over the TA muscle on each rat leg. Each dot

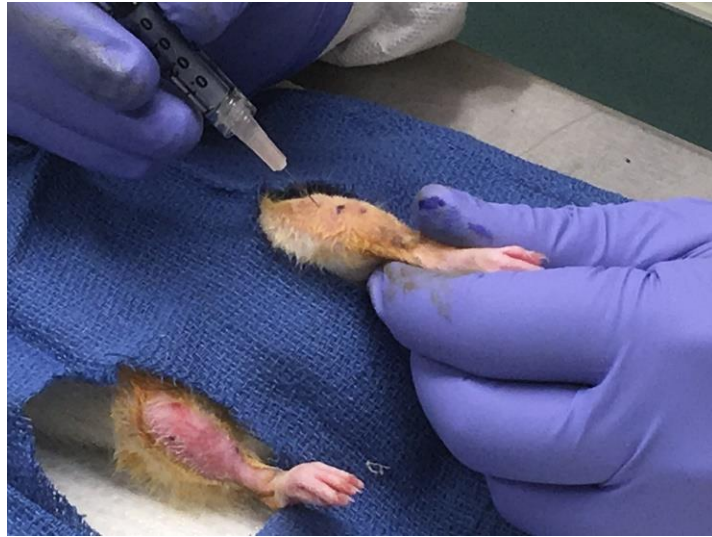marks the site of one of the five 0.1mL injections.

Figure 3 displays the actual surgical procedure: PBS (top) and ECM hydrogel (bottom) injections in the right and left hind TAs, respectively.

Peak Force Normalized to Body Mass
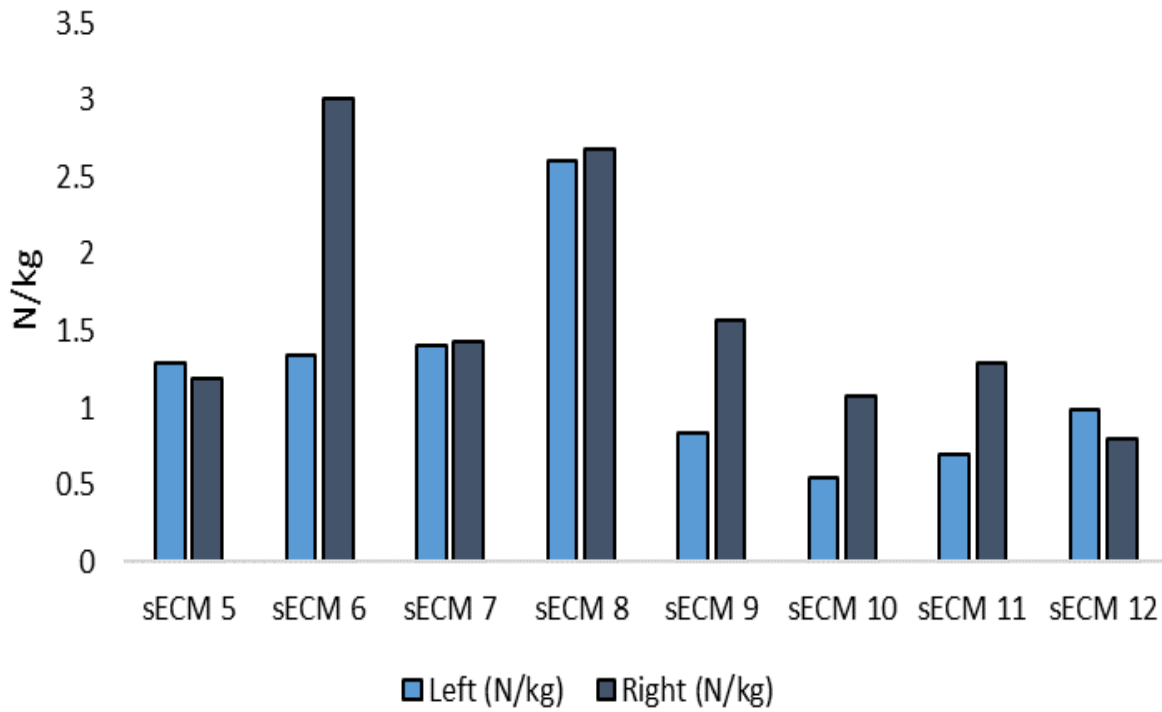
Figure 4 displays peak force for both hind legs of each rat prior to TA harvest, each normalized to the terminal body mass of the rat.

Average Peak Force Normalized to Body Mass
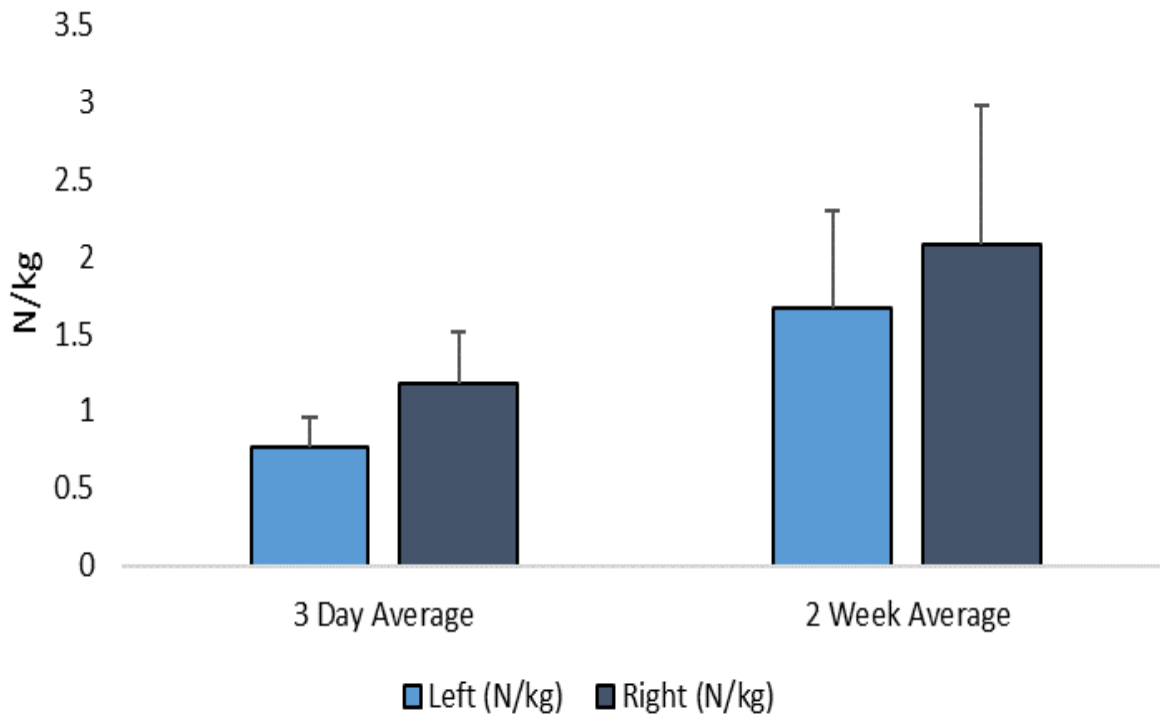
Figure 5 displays the average of peak forces for both hind legs of each rat prior to TA harvest.

Each value is normalized to the terminal body mass of the rat and grouped by leg and timepoint.

*p<0.05 result of Student's two-tailed homoscedastic t-testing.

3 Day Left	3 Day Right	2 Week Left	2 Week Right

1 cm

Figure 6 displays gross TA morphology of representative samples of TAs from both legs and timepoints immediately after harvest. The scale bar in the top left photo applies to all photos in the figure.
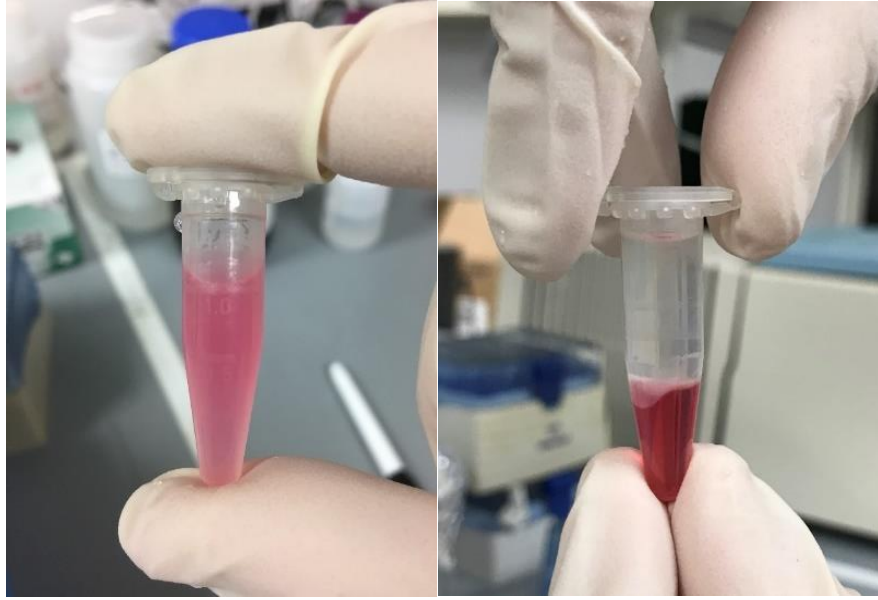
Figure 7 displays the two primary stages of qRT-PCR preparation. Tissue homogenization is shown on the left, and RNA isolation right, with the top clear solution containing the RNA, the middle white solution containing the DNA, and the bottom red solution containing the proteins.
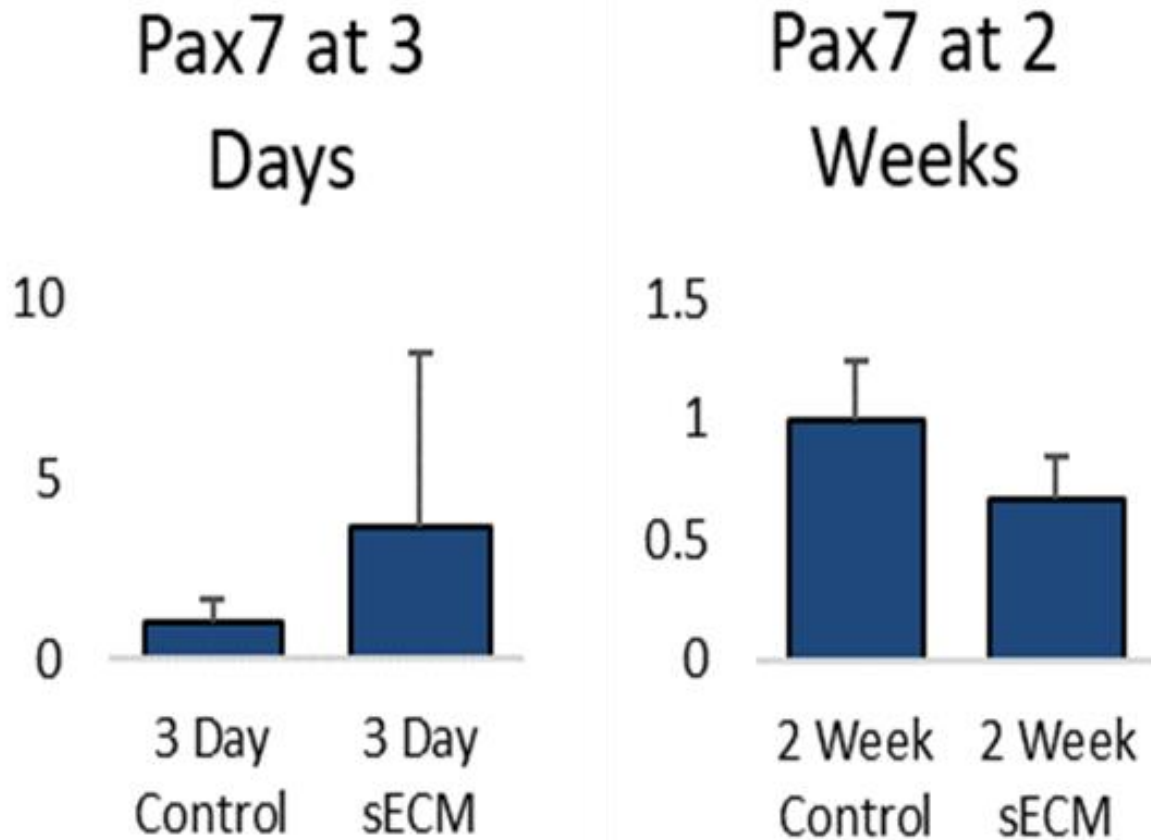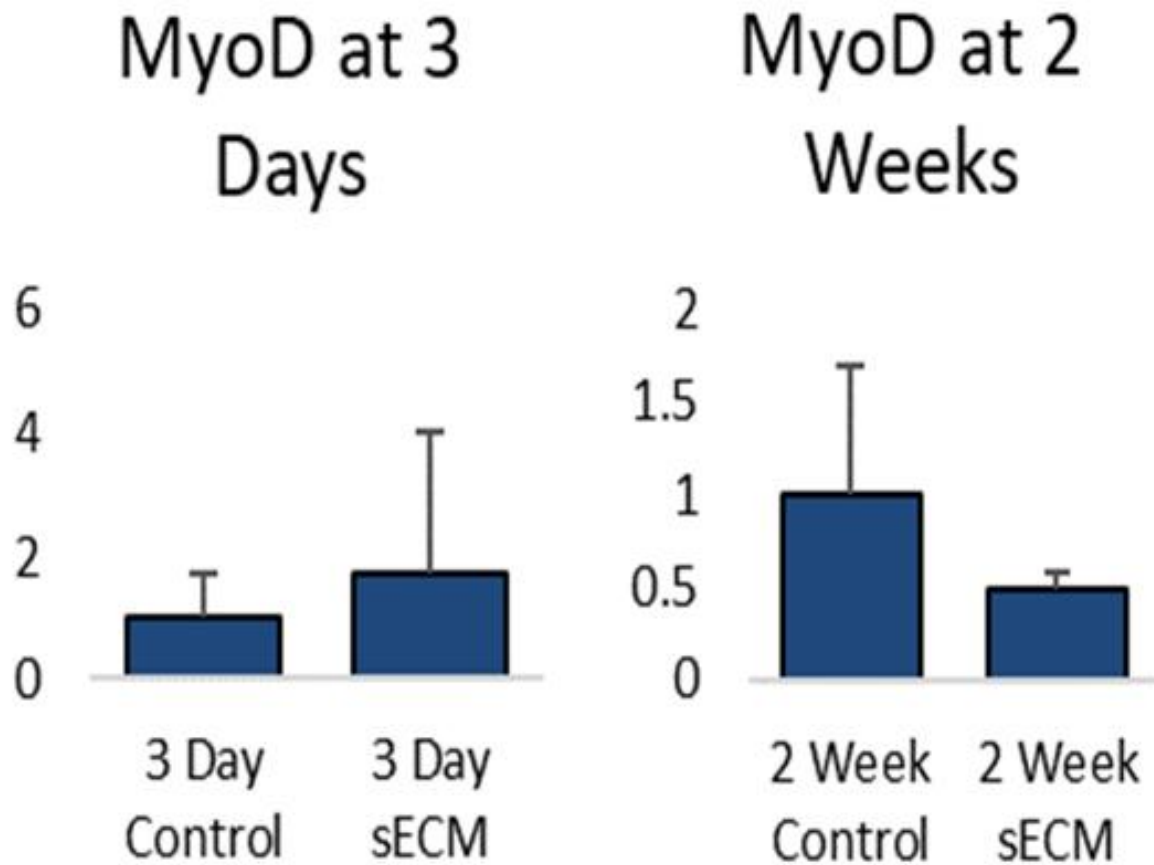
Figure 8 displays qRT-PCR data: gene expression for Pax7 of the myogenic pathway. Values averaged and normalized to the 18s housekeeping gene and to the control group. *p<0.05 result of Student's two-tailed homoscedastic t-testing.
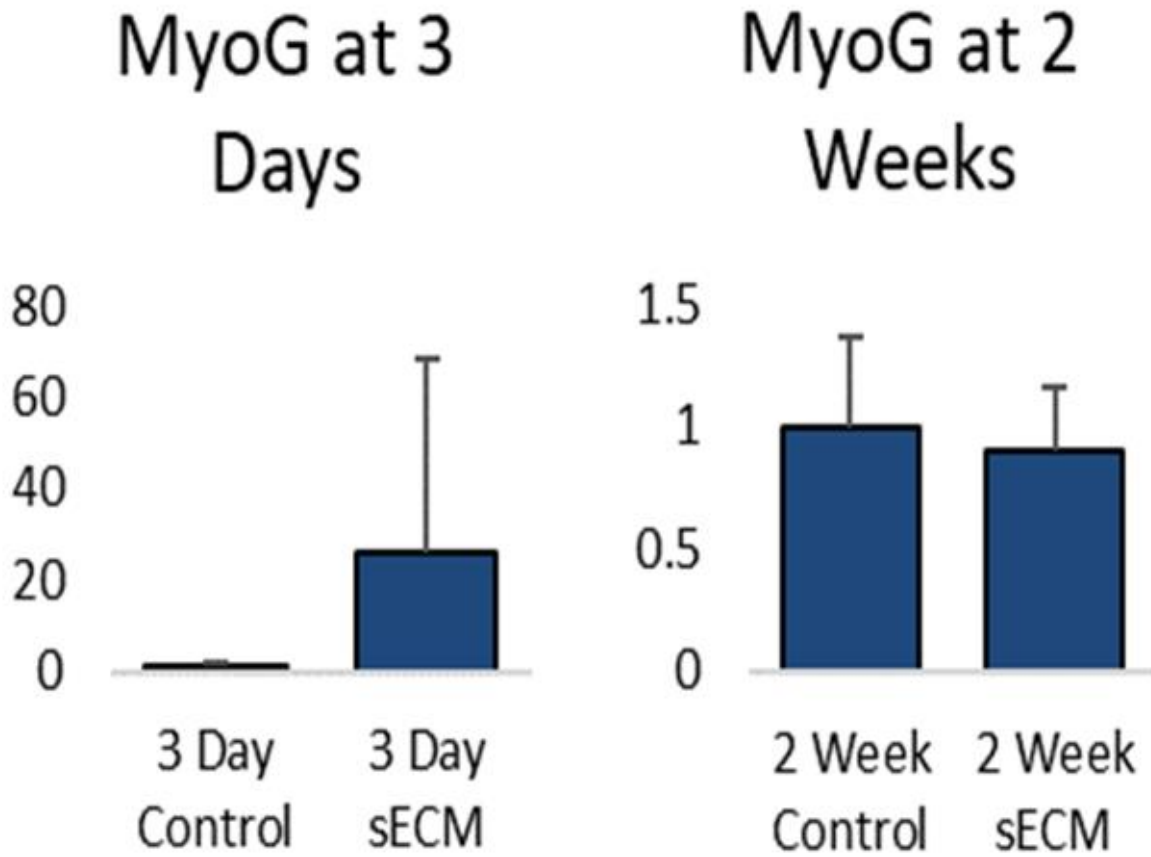
Figure 9 displays qRT-PCR data: gene expression for MyoD of the myogenic pathway. Values averaged and normalized to the 18s housekeeping gene and to the control group. *p<0.05 result of two-tailed homoscedastic t-testing.

Figure 10 displays qRT-PCR data: gene expression for MyoG of the myogenic pathway. Values averaged and normalized to the 18s housekeeping gene and to the control group. *p<0.05 result of Student's two-tailed homoscedastic t-testing.
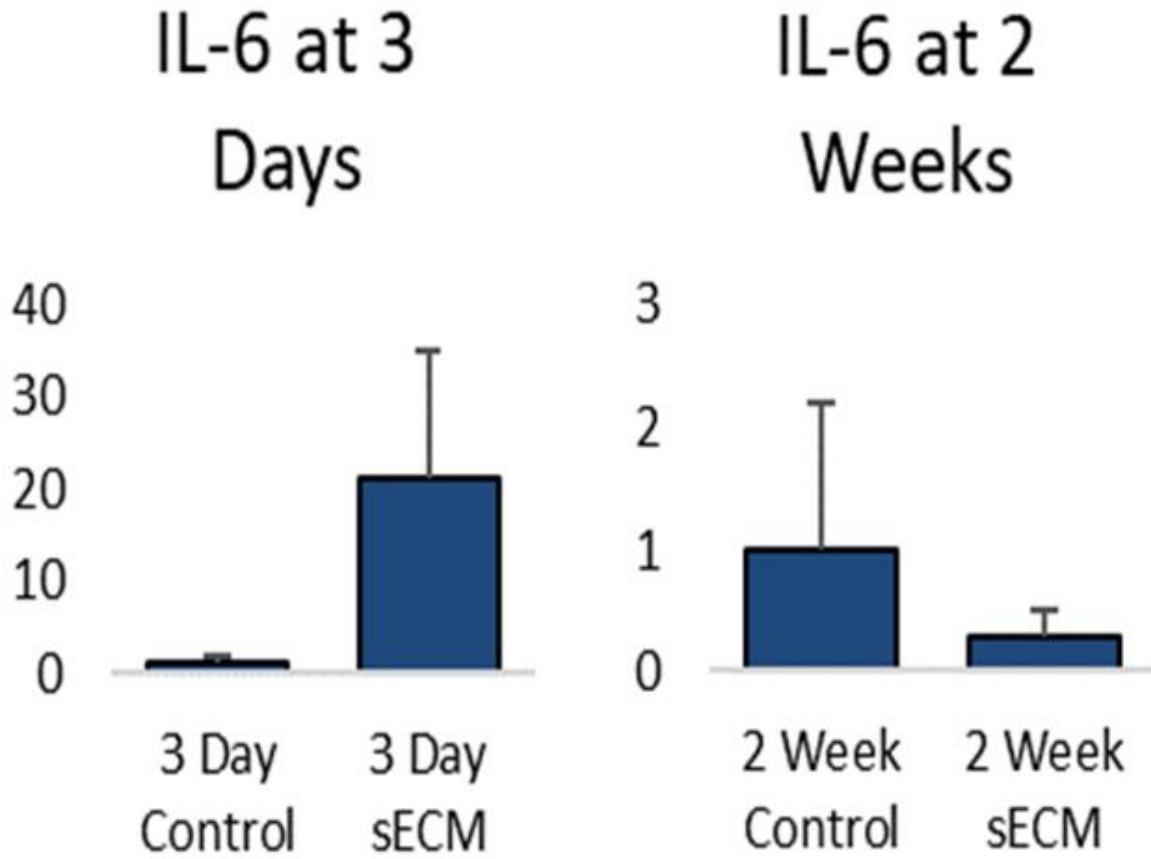
Figure 11 displays qRT-PCR data: gene expression for IL-6 of the inflammatory pathway.

Values averaged and normalized to the 18s housekeeping gene and to the control group. *p<0.05

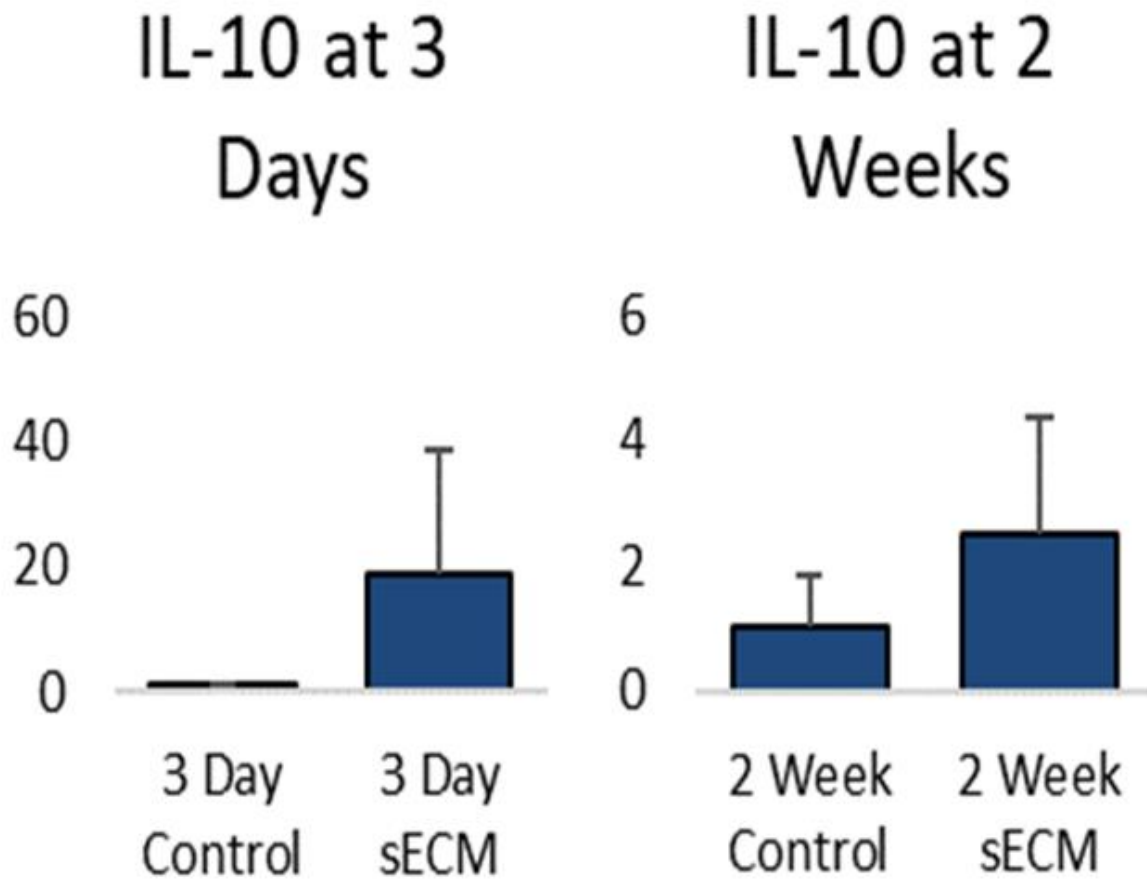result of two-tailed homoscedastic t-testing.

Figure 12 displays qRT-PCR data: gene expression for IL-10 of the inflammatory pathway.

Values averaged and normalized to the 18s housekeeping gene and to the control group. *p<0.05

result of two-tailed homoscedastic t-testing.